Importance of Anharmonicity, Recrossing Effects, and Quantum Mechanical Tunneling in Transition State Theory with Semiclassical Tunneling. A Test Case: The H_2 + Cl Hydrogen Abstraction Reaction†

Jorge A. Sansón, María-Luz Sánchez, and José C. Corchado*

Departamento de Química Física, Facultad de Ciencias, Universidad de Extremadura, Avda. de Elvas S/N, 06071 Badajoz, Spain

Received: May 30, 2005; In Final Form: July 14, 2005

The hydrogen abstraction reaction from H_2 by the Cl atom is studied by means of the variational transition state theory with semiclassical tunneling coefficients on the BW2 potential energy surface. Vibrational anharmonicity and coupling between the bending modes are taken into account. The occurrence of trajectories that recross the transition state is estimated by means of the canonical unified statistical method and by classical trajectories calculations. Different semiclassical methods for tunneling calculations are tested. Our results show that anharmonicity has a small but nonnegligible effect on the thermal rate constants, recrossing can be neglected, and tunneling is adequately described by the least-action approximation, and less successfully by the large-curvature version 3 approximation. However, the large-curvature version 4 and small-curvature approximations lead to a severe underestimation of tunneling. Thermal rate constants calculated using transition state theory including anharmonicity and tunneling agree very well with accurate quantal thermal rate constants over a wide temperature range, although the improvement over the harmonic transition state theory with the microcanonically optimized semiclassical tunneling approximation (based on version 3 of the large-curvature tunneling method) used in a previous study of this reaction is only marginal.

1. Introduction

Variational transition state theory (VTST) with semiclassical tunneling (ST) is one of the most widely used methods for calculating thermal rate constants of polyatomic systems, and the emergence of computer programs that facilitate this kind of calculations, such as Polyrate,[1] Abcrate,[2] or Doit,[3] are popularizing its use. Besides the approximations inherent in the VTST and ST methods, additional approximations are usually made in order to speed up the rate constant calculations, such as considering the vibrational modes to be separable and harmonic.

There is a very large number of studies comparing VTST/ST rate constants with experimental values.[4] The agreement between computed and experimental values is taken as a confirmation of the reliability of the VTST/ST approximation for kinetics studies. However, the quality of the numerical or analytical potential energy surface (PES) employed for the calculation of the rate constants can mask or enhance the validity of the VTST/ST approximations. Hence, it is from the comparison of accurate quantal and VTST/ST rate constants, both obtained using the same PES, that we can learn the most about the soundness of the VTST/ST method. Fortunately, such studies are also abundant,[5−7] leading to the same conclusions: VTST/ST methods can accurately describe the kinetics of most reactions. The quality of the PES also plays an important role in this comparison; only realistic PESs can allow us to conclude whether in real-world settings VTST/ST will behave as expected. Unfortunately, realistic PESs are hard to obtain, and only a small number of them are available.

One of the most realistic PESs is the one by Bian and Werner for the H_2Cl system,[8] denoted as BW2, which has been recently improved to obtain a relativistic PES that includes spin−orbit effects.[9] The latter has been used in the calculation of quantal thermal rate constants explicitly including spin−orbit effects.[10] The authors found that an excellent approximation is to assume that the only effect that spin−orbit coupling has on rate constant calculations is to shift the asymptotic potential energy of the Cl + H_2 reactants. Quantal rate constants calculated under this approximation are available in a wide temperature range.[11] Therefore, the hydrogen abstraction reaction H_2 + Cl → H + HCl on the BW2 PES is a good candidate for testing the accuracy of VTST/ST, which is based on the Born−Oppenheimer approximation and, therefore, can only take into account spin−orbit coupling by changing the asymptotic energy of the reactants.

From the results by Wang and Bian,[12] who used the VTST/ST method under the harmonic approximation for the calculation of thermal rate constants on this PES, we can infer that the VTST/ST method yields results in good agreement with the accurate quantal rate constants by Manthe et al.[11] The goal of the present work is to analyze the influence of different factors which may affect the performance of the VTST/ST methods, particularly (a) vibrational anharmonicity, (b) recrossing of the transition state, and (c) semiclassical tunneling approximations. The choice of an atom−diatom reaction is justified by the fact that the most reliable methods for including vibrational anharmonicity and tunneling effects are only available for triatomic systems. Moreover, accurate quantal rate constants are, with few exceptions, only available for tri- and tetraatomic systems.

The importance of anharmonicity will be the subject of most of our work. The reason is that the majority of the VTST/ST calculations assume that the vibrational modes can be considered as harmonic. Moreover, as we will see below, it will be an

† Part of the special issue "Donald G. Truhlar Festschrift".

10.1021/jp052849d CCC: $33.50
Published on Web 08/23/2005

important factor in the choice of the tunneling method. In addition, we will also analyze several factors that are usually overlooked, such as the numerical stability of the calculations or the importance of quantum effects on the rotational partition functions.

The paper is organized as follows: In section 2, we review some previous work that compares VTST/ST with quantal accurate rate constants, highlighting the results on the $H_2 + Cl \rightarrow H + HCl$ reaction. In section 3, we give an overview of the methods and computational details. In section 4, we show the results of our calculations. The final section presents our conclusions on this reaction.

2. Transition State Theory with Semiclassical Tunneling vs Quantal Rate Constants

As we mentioned in the previous section, the most significant test of VTST/ST is to compare VTST/ST rate constants to rate constants calculated using accurate quantum-mechanical methods on the same PES. The number of such studies is large, starting with the pioneering work of Truhlar and Kuppermann,[5] and up to 1998, they can be summarized by the conclusions of the work by Allison and Truhlar.[7] Their study of 74 atom−diatom reactions can be condensed in their statement that VTST/ST "rate coefficients are generally in excellent agreement with the accurate quantal data". They find that the mean unsigned percentage errors in VTST/ST calculations of thermal rate constants are smaller than 35% all over the temperature range when using the improved canonical variational transition state theory with least-action tunneling (ICVT/LAT) method including vibrational anharmonicity (which is the best method we used in the present work). When they use the harmonic approximation the mean error increases up to 43%.

With respect to the H_2Cl system, their conclusions are in line with these general findings. Thus, when the reaction is assumed to be collinear (one-dimensional) the mean unsigned percentage error of the ICVT/LAT method is smaller than 10%. When the reaction is considered to take place in the three-dimensional world, the differences between VTST/ST and quantal thermal rate constants never exceed 16%.[7,13] Isotopic substitutions do not change these conclusions. However, they found larger discrepancies between VTST/ST and quantal one-dimensional state-selected rate constants. Thus, when H_2 is in its first excited state the ratio between ICVT/LAT and quantal rate constants ranges between 1.90 and 2.34. Isotopic substitution increases this ratio up to 3.57 at 200 K for the perdeuterated state-selected reaction.

Sometimes the comparison between quantal and VTST/ST rate constants has given disappointing results. Thus, studies of the $HCl + O(^3P)$ reaction[14,15] show that the VTST/ST rate constants are much lower than quantal rates at low temperatures, up to a factor of 20 at 200 K, 2.4 at 500 K, and 1.3 at 1000 K. The source of this somewhat surprising result was attributed[15] to resonances found in the cumulative reaction probability, purportedly caused by the influence of van der Waals wells (note that VTST/ST methods are almost insensitive to the presence of these wells). In fact, VTST/ST methods are more prone to fail when these resonances are important at low energies that can have a significant impact on the thermal rate constant. For example, the VTST/ST and quantal rates of this reaction based on an older PES[16] are in better accord,[14] since the quantal cumulative reaction probability shows resonances at high energies that have less effect on the thermal rate constants. It has also been postulated that the reasons behind VTST/ST failure are the importance of bend−stretch coupling and bend-rotation coupling.[14]

Quantal thermal rate constants have been recently available for a more complex system,[17] the hydrogen abstraction reaction $CH_4 + H \rightarrow CH_3 + H_2$, based on the PES by Jordan and Gilbert.[18] This is a good example of the need to compare VTST/ST and quantal results based on the same PES to check the behavior of the VTST/ST methods. The VTST/ST rate constants on Jordan and Gilbert's PES are much higher than experimental rate constants.[19] However, VTST/ST and accurate quantal rates agree within 21% over all of the temperature range investigated.[20] Hence, VTST/ST methods show an excellent performance for this reaction and the discrepancy between experimental and theoretical results is due to deficiencies in the PES.

The same conclusions about the validity of the VTST/ST methods are found in the study of the hydrogen abstraction reaction of $CH_4 + O(^3P)$,[21] which shows that quantal and VTST/ST rate constants agree well (within 50%). In this case, the PES was fitted so that harmonic VTST/ST rate constants reproduce the experimental values;[22] as a consequence, the VTST/ST rate constants are closer to the experimental rates than quantal rates.

Recently Wang and Bian[12] calculated VTST/ST rate constants and kinetic isotope effects for the hydrogen abstraction and exchange reactions in the $H_2 + Cl$ system using the BW2 surface. Their results are in excellent agreement with experimental values, except at high temperatures. When compared with the quantal rate constants of Manthe et al.[11] for the hydrogen abstraction reaction using the same BW2 surface, the low-temperature VTST/ST rate constants as well as the high-temperature rate constants are somewhat greater than the quantal results. For example, VTST/ST rates are 43%, 5%, and 92% greater than the accurate quantal rates at 200, 500, and 1500 K, respectively.

3. Theoretical Methods and Computational Details

Although the VTST/ST methods have been described in many articles and books (see ref 23 and references therein), for the sake of clarity, we will outline them here. Some relevant computational details are also given.

As the first step, one starts locating the reactants and saddle point of the reaction on the PES. The reaction path is initiated at the saddle point by following the imaginary-frequency normal mode eigenvector on each side of the saddle point. Once we have taken the first step on the reaction path, we are no longer in a stationary point and we can follow the gradient direction. Thus, we follow the steepest descent path in isoinertial coordinates[24] all the way to reactants and products. The distance to the saddle point along the reaction path in mass-scaled coordinates is the reaction coordinate, s, which is taken as negative on the reactant side of the reaction path and positive on the product side. The reduced mass used in defining the mass-scaled coordinates was set to the value of the reduced mass of the $H_2 + Cl$ system.

It is not necessary, though, to calculate the entire reaction path all the way to reactants and products; only a fraction of the reaction path is required for VTST calculations. We computed the reaction path over the range between $s = -4$ and $s = +4$ au. The step size for following the gradient was taken to be 0.005 au. These values were checked to be small enough as to give accurate results.

However, such a small step size causes numerical instabilities. For example, in the vicinity of the saddle point the gradients are so small that some magnitudes that are calculated using numerical derivatives of the gradient were found to be quite noisy, especially reaction path curvature components and quartic

bending force constants. To eliminate this noise we apply the moving average method. This way, the vibrational partition functions, vibrational turning points, and reaction path curvature change smoothly all along the reaction path. An alternative is to use sophisticated reaction-path following algorithms which allow much larger step-sizes, as described elsewhere.[25,26] However, since reaction path curvature presents sharp peaks, we require a small step-size to avoid missing these peaks.

Along the reaction path a normal-mode analysis was performed in internal coordinates,[27] projecting out the gradient direction.[28] Having obtained the classical (Born−Oppenheimer) potential energy, geometry, and vibrational frequencies along the reaction path and reactants, we can calculate the rotational moments of inertia and quantal rotational partition functions, vibrational zero-point energies and quantal vibrational partition functions, and the vibrationally adiabatic ground-state potential energy, $V_a^G(s)$, which is defined as the sum of the potential energy and the vibrational zero-point energy, all as a function of the reaction coordinate, s. The maximum of the adiabatic ground-state energy is the threshold energy for the classical reaction probability. Note that we are neglecting rotation−vibration coupling, but we still include coupling between vibrational modes.

The saddle point for this reaction and the geometries along the reaction path are linear. Therefore, there are three bound vibrational modes along the reaction path: a symmetric stretch and a doubly degenerate bend. At this point we neglect the coupling between the stretching mode and the bending modes and we calculate the vibrational partition function as the product of the stretching mode partition function and the doubly degenerate bending modes partition function.

The stretch partition function is computed by summing over the Boltzmann factors of the vibrational energy levels. The ground-state energy is determined by the Wentzel−Kramers−Brillouin (WKB) approximation,[29] but the excited-state energies are determined from the parameters resulting of a Morse fit to the potential.[30]

The coupling between vibrations is expected to be reduced with the use of internal coordinates. In any case, the coupling between the two degenerate bending modes is taken into account by calculating the bend partition function using the centrifugal oscillator model.[31] For comparison, we also calculate the bending mode partition function as the product of two independent vibrational partition functions, one for each bend; the energy levels are determined from a harmonic−quartic potential fit to the true potential.[30,31]

It is important to note that the methods used here are valid if the collinear reaction coordinate is the minimum energy path. In this reaction, however, as we move out of the saddle point in the reactant direction, we approach a T-shaped complex between H_2 and Cl.[11] The reaction path bifurcates; the collinear path becomes a ridge path, the bending potential for collinear geometries is a double well, and two bent minimum energy paths appear, but the reaction-path following algorithm follows the collinear ridge path. Therefore, our anharmonic treatment of the bending modes may be unphysical. Moreover, since we are on a ridge, the bending harmonic frequency is imaginary and the harmonic approach breaks down. Fortunately, the range of the reaction path for which the collinear path is not the minimum energy path is far from the saddle point, having no influence on the rate constant calculation.

Finally, for comparison purposes, we also used the independent normal mode harmonic approximation to compute the vibrational partition functions.

As discussed in ref 10, the spin−orbit splitting lowers the energy of the reactants by 0.84 kcal/mol relative to the reaction path, where spin−orbit splitting is quenched. This can be accomplished by using an appropriate electronic partition function for the Cl reactant that lowers the energy of the reactants by this amount and takes into account the two electronic states of the Cl atom (see eq 13 of ref 11).

The conventional transition state theory (TST) rate constant depends on the ratio of the saddle point partition function to the reactants partition function, as described elsewhere.[30] Note that rotation and vibrations are quantized on the whole reaction path (including reactants), but reaction coordinate motion is not. In this paper, we call this semiclassical.

According to the variational transition state theory, the best transition state is not necessarily at the saddle point. Therefore, we variationally optimize the transition state location by minimizing the semiclassical rate constant with respect to s, which is equivalent to maximizing the free energy of activation, and we call this rate constant canonical variational transition state theory semiclassical rate constant (CVT). Note that the vibrationally adiabatic ground-state potential energy is equivalent to the free energy at 0 K along the reaction path, and that the location of the transition state, $s^{CVT}(T)$, is temperature dependent.

Canonical transition state theory assumes that any molecule which achieves the transition state free energy will break down to products and that systems do not cross energy barriers multiple times. Therefore, if the system recrosses the transition state more than once, transition state theory (at least in the classical world) overestimates the true rate constant. Variational transition state theory optimizes the location of the transition state to minimize recrossing. It is useful to define the variational effect as the ratio of the TST and CVT rate constants, which is equal to or greater than unity, and measures the distance between the optimum transition state and the saddle point.

We can define the recrossing factor (Γ) as the ratio between the number of reactive trajectories and the number of times that the transition state is crossed in the products direction; we assume that this factor is the same as the ratio of the exact rate constant and the transition state rate constant. Thus, the rate constant may be calculated as the product of Γ and the transition state theory rate constant. To estimate the recrossing factor, we ran classical trajectories starting from reactants and products and counted the number of trajectories reaching the products and reactants, respectively, and the number of times that the transition state was crossed. (Since variational effects were found to be very small, we counted the number of times that the saddle point was crossed.) The ratio between them is Γ. The thermal average of energy-dependent recrossing factors is the temperature-dependent recrossing factor. Trajectory calculations were performed using a modified version of the program Mariner,[32] which is a customized version of Venus96.[33]

This kind of calculation is computationally very demanding, especially if an analytical PES is not available. Hence, we calculate the recrossing factor by means of the canonical unified statistical theory (CUS).[34] This method can only be applied if the free energy curve has at least two maxima and the recrossing factor is not very different from unity (the minimum value Γ can have is 0.5). The CUS recrossing factor depends on the ratio between the CVT rate constant and the rate constant calculated at the second maximum of the free energy curve, and also on the ratio between the CVT rate constant and the rate constant calculated at the minumum between the two maxima.[30] The closer the energy of the second maximum is to

the energy of the minimum, the less recrossing it predicts, reaching the $\Gamma = 1$ limit when the second maximum disappears. However, if the energy the two maxima are close in energy and the minimum is significantly lower, Γ approaches 0.5. Thus, if the transition state is located at the maximum closest to reactants, the system may cross the transition state and be trapped at the minimum, from which it stands an equal chance of emerging in either the forward or reverse directions, and $\Gamma = 0.5$.

We also used another method to calculate Γ: the classical dynamical approach based on the reaction path curvature of Miller,[30,35] in its canonical form. This approach assumes that transition state theory is exact below a certain critical energy. According to our calculations the critical energy is at least 12 kcal/mol higher than the energy at the saddle point and canonical recrossing factors are negligibly smaller than unity all over the temperature range. Therefore, we will not discuss these results any further.

To include quantum effects on the reaction coordinate we multiply the semiclassical rate constant by a factor that we call tunneling factor, κ, since tunneling is the dominant quantum effect, although we also take into account the nonclassical reflection. κ is sometimes called transmission factor, but since we are also calculating Γ, the transmission factor in our calculations would be the product of Γ and κ.

A potential barrier is impenetrable to a particle whose energy is lower than the height of the barrier in classical mechanics. However, in quantum mechanics, the probability that the particle passes through the barrier is not zero. This phenomenon is called the tunneling effect. The tunneling probability decreases with the barrier thickness, the barrier height, and increasing mass. Nonclassical reflection is the reflection caused by diffraction from the barrier top even when the energy is above the barrier. If the barrier is assumed to be parabolic in the region near the maximum, then it can be shown semiclassically that for an energy above the barrier by δE, the reflection probability is equal to the tunneling probability for an energy below the barrier by δE. Thus, the reflection probability for energies above the barrier can be calculated from the tunneling probabilities.[30]

In a quantum mechanical world, the lowest energy along the reaction path is the vibrationally adiabatic ground-state potential energy. At low temperatures, where tunneling is most important (the population of the energy levels that are above the barrier to reaction is very small and most of the reaction takes place by tunneling), a quantized system is in its ground state, so that the potential governing the reaction path motion can be taken to be the vibrationally adiabatic ground-state potential energy curve. Therefore, tunneling probability can be calculated as the probability of tunneling through the $V_a^G(s)$ barrier. This is the zero-curvature tunneling (ZCT) method.[36] Note that although we calculate the probability of tunneling through a one-dimensional barrier, we take into account the multidimensional nature of the tunneling effect, since all the vibrational modes contribute to $V_a^G(s)$.

In the absence of reaction path curvature, no internal centrifugal forces would take the system out of the reaction path. However, if the reaction path is curved, the centrifugal forces can move it from the reaction path. In the classically forbidden region the kinetic energy is negative, leading to a negative centrifugal effect. The system moves to the inner side of the reaction path, within the ground-state vibrational amplitude, following a new path, the path of concave-side zero-point energy turning points for the mode coupled to the reaction coordinate by reaction-path curvature, as shown by Marcus and Coltrin[37] for the $H + H_2$ reaction. Here we use a general version of the method that uses a mass for tunneling calculations that depends on the reaction-path curvature, named centrifugal-dominant small-curvature semiclassical adiabatic ground-state tunneling,[38,39] or, for short, small-curvature tunneling (SCT).

When the reaction path curvature is large, the centrifugal forces can push the system beyond the transverse vibrational turning points to a nonadiabatic zone. Hence, the large-curvature tunneling (LCT) methods need to be applied; the most commonly used are LCT versions 3 (LCT3)[38,40] and 4 (LCT4).[41] The LCT methods assume that the tunneling path is a straight line in isoinertial coordinates from the reactant channel to the product channel. The tunneling path is divided into three zones, two of them are in the reactant and product channels, respectively, and they are vibrationally adiabatic, and another zone describes the middle zone of the path and is vibrationally nonadiabatic. Note that for some PESs, the vibrationally nonadiabatic zone does not exist at all energies. It has been noted that the LCT3 method within the harmonic approximation can lead to unphysical resutls:[41] the maximum of the effective potential for tunneling is sometimes lower than the maximum of the $V_a^G(s)$ curve. This is related to errors in the transition between the adiabatic and nonadiabatic regions due to anharmonicity. LCT4[41] includes an anharmonic correction in the vibrationally nonadiabatic region of the tunneling path, calculated as the difference in effective potential energy between adiabatic and nonadiabatic zones computed at the boundary. Since there are two boundaries for each tunneling path with nonadiabatic regions, the anharmonic correction along the nonadiabatic region is obtained by interpolation. Since the LCT4 method was developed to take better account of anharmonicity, it is not useful when anharmonicity is taken into account for the tunneling path calculation. Therefore, it will only be used for LCT calculations under the harmonic approximation.

Note that since LCT methods include a nonadiabatic region, the system enters the tunneling path in its ground state but it can tunnel into vibrational excited states. Nevertheless, we found that in this reaction vibrational excited states were not accessible; only ground-state to ground-state tunneling is energetically allowed.

LCT and SCT tunneling paths are two limit situations: SCT assumes that tunneling is basically in the reaction coordinate direction and the effective tunneling path is at or near the path of outer turning points for the bound vibrational motions coupled by the reaction path curvature to the reaction coordinate, while LCT assumes that the tunneling occurs along the shortest path between the reactant and product channels. However, for a given energy, the SCT tunneling path may be very long and the LCT tunneling path may have a very high barrier. Thus, for systems with intermediate reaction path curvature the optimum tunneling path must be intermediate to the two paths mentioned above. Hence, a method was developed to treat all kinds of systems, based on choosing the best tunneling path from a sequence of paths intermediate to the LCT and SCT paths. Maximum tunneling along the path is equivalent to least imaginary-action integral along the path;[30] this is why this method is called the least-action tunneling method (LAT).[30,42,43]

Although the LAT method is the most accurate of the semiclassical methods usually used along with variational transition state theory, the variational optimization of the tunneling path is a cumbersome procedure, and it is not available for polyatomic systems. Consequently, an approximation to the LAT method called microcanonically optimized multidimensional tunneling (μOMT)[44] is mostly used. It involves comparing

TABLE 1: Conventional Transition State Theory Rate Constants (in $cm^3 \cdot molécule^{-1} \cdot s^{-1}$) for the H_2 + Cl Reaction (in Parentheses, Percentage Deviation from the Fully Anharmonic Results)

T (K)	harmonic	harmonic bends	uncoupled bends	fully anharmonic
150	4.75×10^{-19} (55%)	3.66×10^{-19} (19%)	3.07×10^{-19} (0%)	3.06×10^{-19}
200	5.04×10^{-17} (40%)	4.14×10^{-17} (15%)	3.60×10^{-17} (0%)	3.59×10^{-17}
250	8.31×10^{-16} (33%)	7.10×10^{-16} (13%)	6.29×10^{-16} (0%)	6.26×10^{-16}
300	5.45×10^{-15} (28%)	4.78×10^{-15} (13%)	4.27×10^{-15} (1%)	4.24×10^{-15}
400	5.95×10^{-14} (24%)	5.40×10^{-14} (13%)	4.85×10^{-14} (1%)	4.79×10^{-14}
600	7.32×10^{-13} (22%)	6.88×10^{-13} (15%)	6.12×10^{-13} (2%)	6.00×10^{-13}
800	2.89×10^{-12} (22%)	2.77×10^{-12} (17%)	2.43×10^{-12} (3%)	2.36×10^{-12}
1000	7.19×10^{-12} (24%)	6.96×10^{-12} (20%)	6.00×10^{-12} (3%)	5.81×10^{-12}
1500	2.98×10^{-11} (28%)	2.93×10^{-11} (26%)	2.42×10^{-11} (4%)	2.32×10^{-11}
2100	8.22×10^{-11} (34%)	8.14×10^{-11} (33%)	6.44×10^{-11} (5%)	6.11×10^{-11}

the SCT to the LCT methods and choosing, at each tunneling energy, the one that maximizes the tunneling probability at that energy.

Note that there is an inconsistency in how quantum effects and CVT semiclassical thresholds are handled. The energy threshold for tunneling is given by the maximum of $V_a^G(s)$, being higher than the semiclassical energy threshold for reaction, $V_a^G[s^{CVT}(T)]$. Tunneling occurs at energies below the maximum of $V_a^G(s)$ and classical reaction occurs at energies above $V_a^G[s^{CVT}(T)]$. Therefore, trajectories with total energy between $V_a^G[s^{CVT}(T)]$ and the maximum of $V_a^G(s)$ are counted twice: once in the tunneling calculation and once in the semiclassical CVT calculation. For this reason, we need to eliminate from the transition state partition functions the contribution from below the vibrationally adiabatic ground-state threshold, obtaining improved partition functions.[45] Using these improved partition functions we calculate the improved CVT (ICVT)[45] rate constants. In our calculations, the ICVT results are within 2% of the results obtained with the microcanonical version of the variational transition state theory.[30]

All the VTST/ST calculations were carried out using Polyrate[1] and a locally modified version of Abcrate.[2]

4. Results

4.1. Semiclassical Rate Constants. We start by analyzing a factor that is usually overlooked: quantum effects on rotations. Since rotational levels are closely spaced, rotational partition functions are frequently calculated using classical mechanics. We find that, at the lowest temperature under study, 150 K, the quantum and classical rotational partition functions of the saddle point differ only by 3% and above 500 K they differ by less than 1%. However, the quantum mechanical partition function of the H_2 reactant is higher than its classical counterpart by 22% at 150 K, 10% at 300 K, and 5% at 600 K. Therefore, neglecting quantum effects on H_2 rotation causes low temperature rate constants to be overestimated by up to 18% at 150 K. Thus, rotational partition functions are treated quantum mechanically in the rest of the paper.

Since vibrational energy levels are discrete, the vibrational partition functions are calculated quantum mechanically. For the sake of clarity, we start by analyzing the effects of anharmonicity on the semiclassical conventional transition state theory rate constants (TST). Table 1 lists the TST rate constants calculated with harmonic vibrational zero-point energies and partition functions (second column), TST rate constants including anharmonic contributions from the stretching mode (third column), TST rate constants assuming that the stretching and bending modes are separable anharmonic oscillators (fourth column), and the TST rate constants using the WKB approximation to treat the ground-state vibrational stretch, the Morse approximation for excited states of the stretch, and the centrifugal oscillator approximation for the bends (fifth column). Table 1 shows that the coupling between the two bending modes has a very small effect on the rates: columns four and five differ by less than 5%. However, the effect of treating the bending modes as separable harmonic vibrators is significant: the rate constants in column three are around 20% higher than the fully anharmonic rates. This effect is more pronounced at both edges of the temperature range. The largest difference is found at high temperatures (33% at 2100 K). Finally, the effect of anharmonicity on the vibrational stretch diminishes as temperature increases, so that the difference between the fully harmonic and the fully anharmonic rate constants at 2100 K is due to the anharmonicity of the bending modes. Table 1 also shows that above 400 K stretch anharmonicity changes the rate constants by less than 10%. Therefore, stretch anharmonicity is significant only at low temperatures.

In brief, fully harmonic rate constants (second column) are higher than fully anharmonic rate constants (fifth column) by less than 30% over the temperature range from 300 to 1500 K. Therefore, the harmonic approximation works reasonably well for semiclassical TST.

Anharmonicity of the stretching mode deserves further study. The two bending modes evolve into free rotations or translations at reactants and products, but the symmetric stretch of the saddle point evolve into the H_2 stretching mode at reactants. The stretch partition function of the saddle point is in the numerator of the rate constant expression, and the H_2 stretch partition function is in the denominator. Therefore, the small effect of vibrational anharmonicity on the rate constant may be due to the validity of the harmonic oscillator model, or to the fact that the saddle point stretch anharmonicity is partially canceled by the H_2 anharmonicity.

At 200 K the value of the anharmonic vibrational partition function of H_2 is 1.61×10^{-7}, while its harmonic counterpart is 20% lower, 1.29×10^{-7}. At 1500 K, they are 0.126 and 0.122 respectively; they differ by less than 3%. With respect to the saddle point, the values of the 200 K anharmonic and harmonic stretch partition functions are 7.67×10^{-3} and 7.50×10^{-3}, respectively, while at 1500 K they are 0.726 and 0.715; the difference is around 2%, and it is almost independent of temperature. Hence, the harmonic approximation works very well for the stretching mode of the saddle point, and reasonably well for the H_2 stretch. Moreover, most of the differences between harmonic and anharmonic TST rate constants at low temperatures are due to the anharmonicity of the H_2 vibrational stretch.

As we mentioned above, only the ground state energy of the stretching mode is computed by the WKB method based on the true potential, and the excited states are calculated from a Morse fit. Since stretching vibrational frequencies are relatively high (4409 cm^{-1} at reactants and 1360 cm^{-1} at the saddle point),

the population of excited states is very small over the temperature range under study. Therefore, the choice of the model for describing the excited states is expected to have little effect on the vibrational partition functions. Thus, the use of the harmonic approximation instead of the Morse model reduces the partition function of the saddle point by only 1.5% at 1500 K, the differences at lower temperatures are negligible, and the H_2 partition function is almost unaffected. We can therefore conclude that it suffices to treat the ground state of vibrational stretch accurately to include most of the anharmonicity effects on stretches.

After studying the importance of anharmonicity on conventional transition state, we proceed to analyze variational transition state theory calculations. It has to be noted that our study on the effects of anharmonicity based on the saddle point are applicable here, since variational effects are very small over all the temperature range. As temperature increases, the optimum transition state moves toward products, but it does it so slowly that anharmonic conventional and variational transition state theory rate constants agree within 1%. Under the harmonic approximation, the variational effects are slightly larger; the harmonic TST rate constants are 18% higher than the harmonic ICVT results at 150 K, and the transition state is located on the reactant side of the reaction path. As temperature increases, the transition state moves in the product direction, getting closer to the saddle point; variational effects vanish (3% at 200 K, and less than 1% above 400 K).

Looking at the harmonic and anharmonic zero-point energies, we find that the contribution from bending modes is smaller under the harmonic approximation. In both cases, it reaches a maximum at the saddle point and the motion along the reaction coordinate leads to a larger decrease of the zero-point energy of the bending modes when they are treated as anharmonic coupled oscillators. The contribution from the stretching mode is very similar whether we use the harmonic or anharmonic results for the saddle point, as we discussed above. The zero point energy of the stretch has a minimum at the saddle point and the motion along the reaction coordinate leads to a larger increase of the zero-point energy of the stretching mode when it is treated as a harmonic oscillator.

At low temperatures, as we start descending from the saddle point to reactants, we find that, near the saddle point, the decrease in free energy due to the contributions of the harmonic bending modes and the classical potential energy is smaller than the increase in free energy due to the contribution of the harmonic stretching mode. Thus, the harmonic transition state at low temperatures is located on the reactant side of the reaction path ($s^{CVT} = -0.3$ au at 0 K) because of the changes in the stretching mode frequency. On the other hand, as the temperature increases the contribution of the bending modes becomes more significant. As a result, the transition state approaches the saddle point location, since the harmonic frequency of the bending modes peaks near the saddle point. So, variational effects computed under the harmonic approximation are significant only at very low temperatures.

Conversely, the factor that controls the location of the transition state under an anharmonic approximation is the contibution of the bending modes. The reason is the contribution of the quartic terms which also reach their maximum in the saddle point zone. This is why the variational effects on anharmonic semiclassical rate constants are negligible.

Therefore, although harmonic calculations overestimate the conventional TST rate constants, this overestimation is partially compensated by variational effects. As a result, harmonic ICVT rate constants give better agreement with anharmonic ICVT rate constants than their conventional TST counterparts. Thus, the greatest difference between harmonic and anharmonic rates is 36% at 200 K.

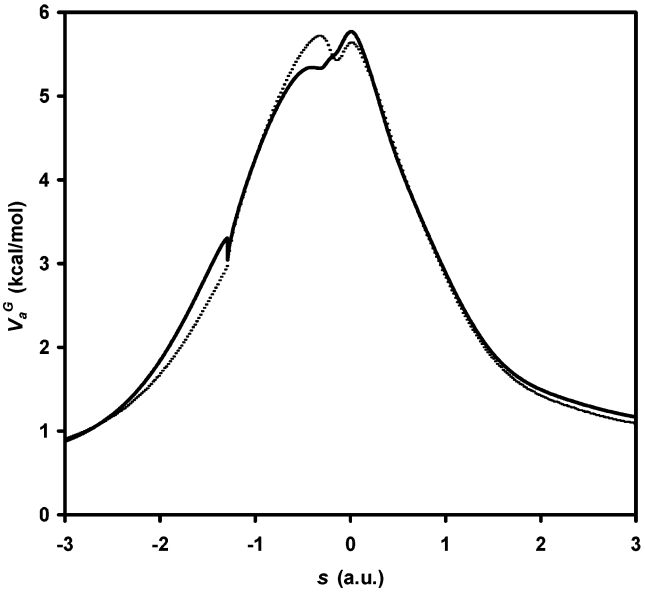

Figure 1. Vibrationally adiabatic ground-state potential energy, $V_a^G(s)$. The solid line is based on anharmonic zero-point energies, and the dotted line is based on harmonic zero-point energies.

4.2. Recrossing Factors. Transition state theory implies the assumption of no recrossing trajectories that would lead to an overestimation of the rates by the statistical rate theory. This assumption is usually fulfilled for bimolecular gas-phase reactions, when the free energy along the reaction path has only one maximum. However, the free energy along the $Cl + H_2$ reaction path presents two maxima near the saddle point. Figure 1 shows the vibrationally adiabatic ground-state potential energy along the reaction path (which is equivalent to the free energy of activation at 0 K) calculated using harmonic and anharmonic vibrational zero-point energies. The anharmonic energy shows a global maximum at the saddle point, and a local maximum 0.3 kcal/mol lower in energy than the global one, on the reactant side, at $s = -0.3$ au. In opposition, harmonic calculations predict the latter to be the global maximum, although the former is almost equally high. It has to be noted that the different shape of the two energy curves is due to the above-mentioned fact that the harmonic bending energy is lower than the anharmonic bending energy at $s = -0.3$ au, while the harmonic stretching energy is higher than its anharmonic counterpart.

The presence of a second maximum near the transition state may be responsible for some transition state recrossing. Trajectories may be trapped in the minimum between the two maxima, crossing the transition state several times before reverting to reactants or evolving to products. Since the minimum is close in energy to the lowest maximum, it seems difficult to trap trajectories long enough to originate a significant recrossing of the transition state. This is especially true for anharmonic calculations, which give almost the same energy for the lowest maximum and the minimum. Thus, recrossing effects are expected to be negligible.

To check this assumption, we calculated recrossing factors using two methods, besides Miller's classical canonical correction[35] discussed previously: the canonical unified statistical (CUS) theory and a statistical analysis of classical trajectories.

The CUS method with anharmonic vibrations predicts recrossing factors very close to unity. For temperatures below

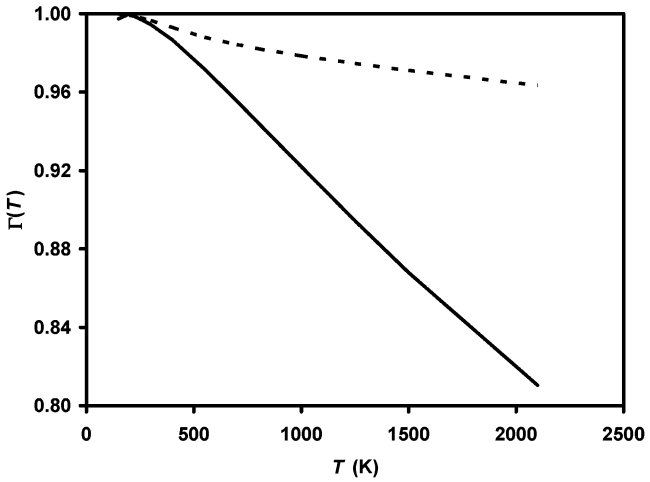

Figure 2. Recrossing factor, $\Gamma(T)$. The solid line is the canonical unified statistical theory calculation, and the dotted line is the classical trajectories calculation.

400 K the recrossing factor, Γ, is higher than 0.99, and it slightly diminishes as temperature increases. The lowest value that we found for Γ is 0.81 at 2100 K. The reason is that the two maxima of the free energy become more similar to one another as the temperature increases.

However, when we assume that vibrations are harmonic we find that the higher the temperature, the closer to unity the value of Γ. The reason is that at high temperatures the maximum at $s = -0.3$ au disappears, giving rise to a single maximum for the harmonic free energy profile located at the saddle point ($s = 0.0$ au). Thus, the harmonic CUS factor is higher than 0.99 at temperatures above 600 K, and the lowest value for Γ is found at 150 K ($\Gamma = 0.70$).

We also obtained Γ by running classical trajectories from reactants to products and viceversa; the temperature-dependent Γ is the thermal average of the energy-dependent recrossing factor for each trajectory. (The transition state was assumed to be located at the saddle point for all the trajectories.) We found that the energy-dependent recrossing factor is higher than 0.99 for most of the thermally accessible trajectories below 400 K and lower than 0.90 only at very high total energies, whose contribution to the reactivity below 1500 K is smaller than 1%. As a result, the thermally averaged recrossing factors are closer to unity than the anharmonic CUS factors. Thus, the lowest value we obtained from trajectories is $\Gamma = 0.96$ at 2100 K. Although in both cases Γ increases with temperature, the temperature dependence predicted by classical trajectories is weaker, as seen in Figure 2. Note that harmonic CUS factors predict the opposite temperature dependence. In brief, anharmonic CUS and classical trajectories recrossing factors differ appreciably (at 2100 K the overestimation rate constant by the CVT method is 19% according to the anharmonic CUS approximation and only 4% according to classical trajectories); however, in both cases recrossing has little influence on the rate constant (less than 20% at 2100 K, and less than 14% at 1500 K). Consequently, we will assume that recrossing effects can be neglected.

4.3. Tunneling Factors. Tunneling factors include two quantum effects: tunneling and overbarrier nonclassical reflection. The latter was calculated using zero-curvature tunneling (ZCT) probabilities and the parabolic approximation described above. Underbarrier tunneling probabilities were calculated using the small-curvature tunneling (SCT) approach, the large-curvature tunneling (LCT) approach versions 3 (LCT3) and 4 (LCT4), and the least-action tunneling approach (LAT). LCT3 was used with the harmonic and anharmonic approximations for vibrations, while LCT4 was used only with harmonic vibrations. The tunneling factors are listed in Tables 2 and 3.

TABLE 2: Semiclassical Tunneling Coefficients Calculated Using the Small-Curvature Tunneling (SCT), Large-Curvature Tunneling Version 3 (LCT3), Microcanonically Optimized Multidimensional Tunneling (μOMT), and Least-Action Tunneling (LAT) Methods with Anharmonic Vibrations

T (K)	SCT	LCT3	μOMT	LAT
150	23.76	22.24	27.91	44.46
200	6.40	7.16	7.78	9.99
250	3.42	3.98	4.14	4.82
300	2.40	2.81	2.87	3.19
400	1.66	1.92	1.94	2.06
600	1.26	1.42	1.42	1.46
800	1.14	1.26	1.26	1.28
1000	1.09	1.18	1.18	1.20
1500	1.04	1.10	1.10	1.11
2100	1.02	1.06	1.07	1.07

TABLE 3: Semiclassical Tunneling Coefficients Calculated Using the Small-Curvature Tunneling (SCT), Large-Curvature Tunneling Version 3 (LCT3), Large-Curvature Tunneling Version 4 (LCT4), Microcanonically Optimized Multidimensional Tunneling Based on LCT3 (μOMT3), Microcanonically Optimized Multidimensional Tunneling Based on LCT4 (μOMT4), and Least-Action Tunneling (LAT) Methods with Harmonic Vibrations

T (K)	SCT	LCT3	μOMT3	LCT4	μOMT4	LAT
150	12.54	23.73	24.58	9.25	13.45	41.72
200	3.88	7.43	7.49	3.65	4.23	9.68
250	2.34	4.08	4.09	2.34	2.52	4.75
300	1.79	2.86	2.87	1.83	1.91	3.16
400	1.38	1.95	1.95	1.41	1.44	2.06
600	1.15	1.44	1.44	1.17	1.18	1.47
800	1.08	1.27	1.27	1.09	1.10	1.29
1000	1.05	1.19	1.19	1.06	1.06	1.21
1500	1.02	1.11	1.11	1.03	1.03	1.12
2100	1.01	1.07	1.07	1.01	1.01	1.08

From Table 2 we can see that at 150 K tunneling mostly takes place through tunneling paths intermediate to the LCT3 path and the SCT path. Thus, at 150 K, the LAT tunneling factor is about twice the values of the SCT and LCT3 factors. As energy increases, the dominant tunneling paths approach the LCT3 paths, so that LCT3 is larger than SCT above 200 K, and the optimum tunneling paths are the LCT3 paths for most of the energies.

As a consequence of the above, the microcanonically optimized multidimensional tunneling approach (μOMT) cannot provide an adequate description of low-energy tunneling, since optimum tunneling paths are neither SCT nor LCT3 tunneling paths. Thus, μOMT tunneling factors at 150 K are significantly lower than LAT factors. However, since LCT3 paths are close to the high-energy optimum tunneling paths, the difference between the LAT and μOMT factors diminishes rapidly as temperature increases, being less than 15% at 250 K.

As mentioned above, LCT4 was developed to solve problems related to the harmonic approximation; therefore, we did not use LCT4 tunneling when anharmonicity was included. In any case, we checked that LCT3 and LCT4 methods predict the same boundaries between adiabatic and nonadiabatic zones, and that the LCT4 anharmonic correction to the effective potential for tunneling was zero. Therefore, anharmonic LCT3 and anharmonic LCT4 methods give the same results.

Table 3 shows the tunneling factors calculated under the harmonic approximation. Note that the SCT tunneling factors

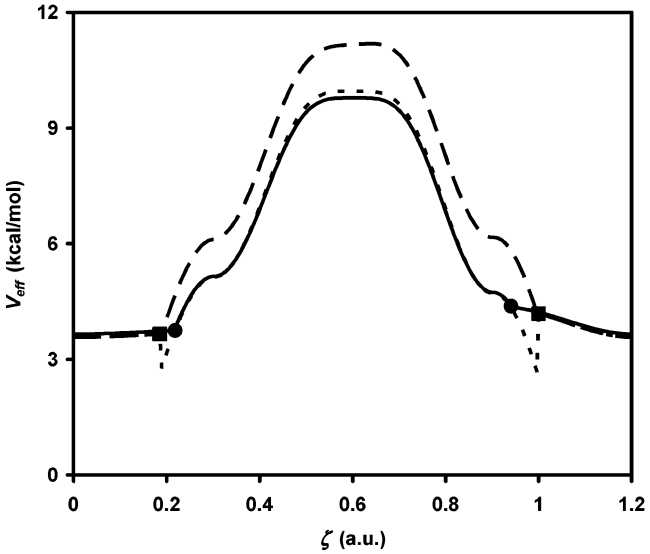

Figure 3. Effective potential for tunneling calculated using the anharmonic LCT3 method (solid line), harmonic LCT3 method (dotted line), and harmonic LCT4 method (dashed line). The location of the adiabatic/nonadiabatic boundaries are also shown (anharmonic LCT3, solid circles; harmonic LCT3 and LCT4, solid squares). The energy of the tunneling path is 2.1 kcal/mol below the energy of the adiabatic barrier.

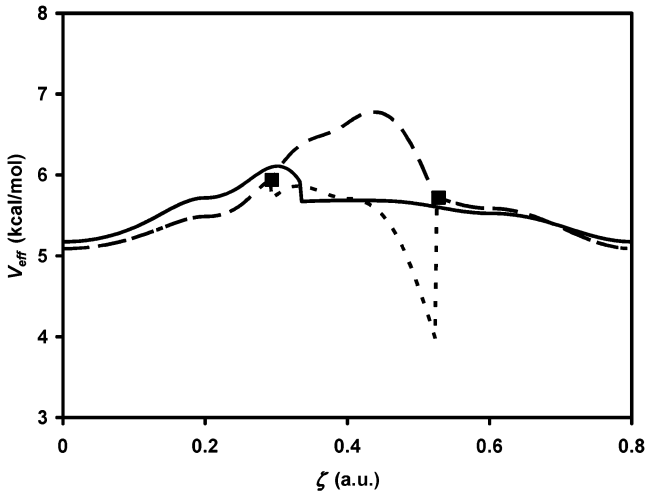

Figure 4. Effective potential for tunneling calculated using the anharmonic LCT3 method (solid line), harmonic LCT3 method (dotted line), and harmonic LCT4 method (dashed line). The location of the adiabatic/nonadiabatic boundaries for harmonic LCT3 and LCT4 calculations are also shown (solid squares). The energy of the tunneling path is 0.9 kcal/mol below the energy of the adiabatic barrier.

are smaller than the LCT3 ones, so that μOMT factors based on LCT3 are very close to LCT3 factors. Moreover, the μOMT method predicts smaller tunneling factors than the LAT method, the differences being slightly smaller than those obtained from anharmonic calculations. The lower values obtained for harmonic SCT coefficients when compared to the anharmonic SCT results can be explained by the shape of the $V_a^G(s)$ curve near the saddle point, which is thinner for the anharmonic case, since the same behavior is also found in the ZCT factor (not shown here).

LCT4 predicts much lower tunneling factors, less than half the LCT3 factors. This is the expected behavior, because LCT4 was devised to reduce the overestimation of the LCT3 tunneling caused by the harmonic approximation. However, if we compare the anharmonic LCT3 calculations (which are supposed to be more accurate), to harmonic LCT3 and harmonic LCT4 results, the harmonic LCT4 method seems to severely underestimate tunneling effect. The harmonic LCT3 factors are larger than the anharmonic LCT3, as expected, but the differences are less than 7% at 150 K, and they diminish as temperature increases. However, the LCT4 values at 150 K are about half those obtained with the anharmonic LCT3 method.

The reason for this underestimation of tunneling by the LCT4 method can be seen in Figures 3 and 4. Harmonic LCT3 locates the boundaries of the nonadiabatic zone (shown as filled squares) too close to the reaction path, as compared to the anharmonic LCT3 boundaries (shown as filled circles in Figures 3 and 4). The nonadiabatic region is larger and the adiabatic regions are shorter when vibrations are harmonic. Therefore, when vibrations are treated harmonically, some regions along the tunneling path are treated as if they were nonadiabatic, but they are adiabatic. The LCT3 effective potential for tunneling in these regions is too low and it shows discontinuities at the boundaries. However, when both harmonic and anharmonic LCT3 methods consider the point to be in the nonadiabatic region, the two approaches give similar values for the effective potential for tunneling. Hence, the harmonic LCT3 approximation produces unphysical results in the fragment of the tunneling path considered to be in the nonadiabatic zone that the anharmonic approximation locates in the adiabatic zone.

The LCT4 method minimizes the discontinuity due to the transition between the adiabatic and nonadiabatic region by adding a correction potential that accounts for the anharmonicity of the vibrations. Note that in our calculations the LCT4 anharmonic correction is always positive and, therefore, the LCT4 and LCT3 adiabatic/nonadiabatic boundaries coincide[41] (shown as filled squares in Figures 3 and 4). The LCT4 anharmonic correction is computed as the difference between the adiabatic effective potential and the nonadiabatic effective potential at the boundaries, and it is linearly interpolated along the nonadiabatic region of the tunneling path. Since the correction is large and positive, it significantly increases the height of the barrier to tunnel through. Thus, the LCT4 path is much higher in energy than either the harmonic or anharmonic LCT3 paths and, therefore, LCT4 tunneling probabilities are much lower than those from anharmonic LCT3 calculations.

Harmonic LCT3 probabilities are very close to the anharmonic LCT3 ones, although the former are slightly higher at low energies (because a small fraction of the barrier is removed), and at high energies. In fact, LCT4 was developed to correct the fact that according to the harmonic LCT3 approach the reaction can have a region where the maximum of the effective potential along the tunneling path is lower than the maximum of the vibrationally adiabatic ground-state potential. As seen in Figure 4 for a high-energy case, the anharmonic LCT3 path entirely lies within the adiabatic region, but the harmonic LCT3 path has a nonadiabatic zone. The effective potential in this zone erroneously taken as a nonadiabatic zone is too low, as we saw in Figure 3 for a low-energy tunneling path. Therefore, the maximum of the effective potential along this tunneling path is at the adiabatic/nonadiabatic boundary, and it may be lower than the maximum of the vibrationally adiabatic potential. As a result, high-energies harmonic LCT3 tunneling probabilities are higher than the anharmonic LCT3 probabilities. To correct this deficiency, the LCT4 method adds a term that makes the effective potential much higher than the anharmonic LCT3 one.

Therefore, for this reaction, the LCT4 method overcorrects the harmonic LCT3 results because it increases the potential of the whole harmonic LCT3 nonadiabatic region, which is in

TABLE 4: Variational Transition State Theory and Quantal Rate Constants (in $cm^3 \cdot molecule^{-1} \cdot s^{-1}$) for the $H_2 + Cl$ Reaction (in Parentheses, Percentage Deviation from the Accurate Quantal Results)

T (K)	ICVT/LAT	CUS/LAT	harmonic ICVT/LAT	quantal[a]
150	1.36×10^{-17} (44%)	1.35×10^{-17} (43%)	1.68×10^{-17} (78%)	9.45×10^{-18}
200	3.58×10^{-16} (28%)	3.58×10^{-16} (28%)	4.72×10^{-16} (63%)	2.89×10^{-16}
250	3.01×10^{-15} (8%)	3.00×10^{-15} (8%)	3.89×10^{-15} (39%)	2.79×10^{-15}
300	1.35×10^{-14} (−1%)	1.34×10^{-14} (−1%)	1.71×10^{-14} (25%)	1.36×10^{-14}
400	9.84×10^{-14} (−8%)	9.71×10^{-14} (−10%)	1.22×10^{-13} (13%)	1.07×10^{-13}
600	8.76×10^{-13} (−9%)	8.47×10^{-13} (−12%)	1.07×10^{-12} (12%)	9.59×10^{-13}
800	3.02×10^{-12} (−2%)	2.85×10^{-12} (−7%)	3.72×10^{-12} (21%)	3.07×10^{-12}
1000	6.94×10^{-12} (9%)	6.40×10^{-12} (1%)	8.65×10^{-12} (36%)	6.34×10^{-12}
1500	2.57×10^{-11} (55%)	2.23×10^{-11} (35%)	3.32×10^{-11} (100%)	1.66×10^{-11}
2100	6.53×10^{-11}	5.29×10^{-11}	8.81×10^{-11}	
mean error	16%	12%	40%	

[a] Reference 11.

general in good agreement with the anharmonic LCT3 nonadiabatic potential, instead of correcting only the region where harmonic LCT3 gives unphysical values of the effective potential. In fact, it seems that the problems of the harmonic LCT3 method are related to the location of the boundaries between the adiabatic and nonadiabatic zones, rather than to the calculation of the effective potential for tunneling along the nonadiabatic region. Thus, if we use the anharmonic LCT3 adiabatic regions and the harmonic LCT3 nonadiabatic region, the results are very close to those obtained with the fully anharmonic LCT3. Conversely, if we use the anharmonic LCT3 adiabatic regions and the harmonic LCT4 nonadiabatic region, the barrier to tunnel through is too high and tunneling is underestimated. Hence, the LCT4 method, which is based on correcting the energy of the nonadiabatic region, is inadequate at least for this reaction.

4.4. Comparison with Accurate Quantal Rate Constants. According to our previous discussions, our best values of the rate constants are those obtained from the ahnarmonic ICVT/LAT calculations. In Table 4, we compare these results to those by Manthe et al.[11] We also check the performance of the anharmonic CUS/LAT and harmonic ICVT/LAT methods. Figures 5 and 6 compare our ICVT/LAT values with the results from ref 11 and the harmonic ICVT/μOMT results (based on classical rotational partition functions) by Wang and Bian.[12] Note that the latter are very close to our harmonic ICVT/LAT results, since over the temperature range studied in ref 12, LAT and μOMT (based on LCT3) tunneling factors are very close each other and quantum effects on rotational partition functions are very small.

From Figure 6, it can be seen that the differences between VTST/ST and accurate rates are about 50% smaller when anharmonicity is included. However, in Figure 5 it can be seen that the harmonic results from ref 12 are very similar to both our anharmonic ICVT/LAT calculations and accurate quantum mechanical results. The agreement between the harmonic results by Wang and Bian and our more accurate results is partially due to a compensation of different errors: the underestimation of the contribution of the bends is compensated by the overestimation of the contribution of the stretch; the underestimation of tunneling by the μOMT method is compensated by the overestimation of the low-temperature rate constants due to the use of classical partition functions for rotations and the harmonic approximation for vibrations. However, as we have seen all throughout the paper, the errors are relatively small, and although the harmonic results benefit from some fortunate error cancellation, the harmonic ICVT/μOMT rates are close to the accurate ones because the reaction is adequately described by the harmonic VTST/ST methods.

From Figure 5, it can be seen that our values exhibit a more pronounced curvature in the Arrhenius plot than the quantal values. We believe that the reason for the overestimation of low-temperature rate constants is the overestimation of tunneling effects, while the high-temperature deviation could be due to anharmonicity, vibrational coupling (or rotational−vibrational coupling), and transition state recrossing, as seen by the fact that CUS/LAT rates agree better with accurate results (Figure 6).

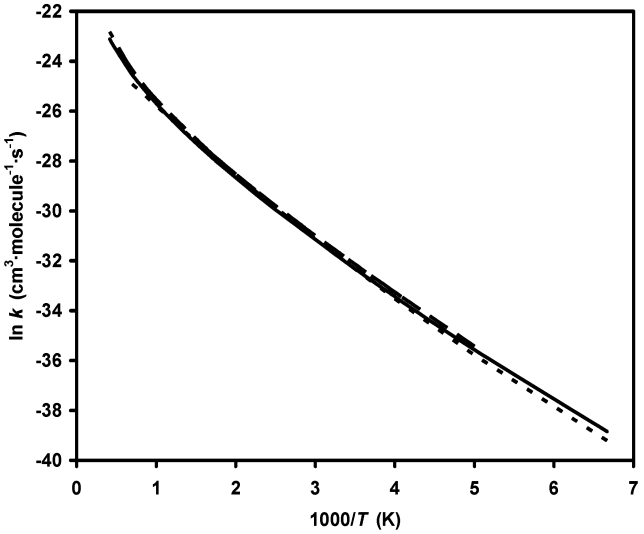

Figure 5. Arrhenius plot of the rate constants of the $H_2 + Cl$ reaction. The solid line denotes the ICVT/LAT values. The dashed line is the harmonic ICVT/μOMT values from ref 12. The dotted line is the accurate quantal results from ref 11.

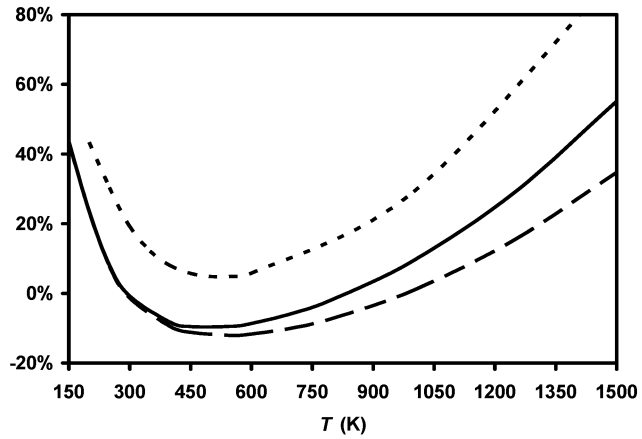

Figure 6. Percentage deviation from accurate quantal results. The solid line is the ICVT/LAT values, the dahed line is the CUS/LAT values, and the dotted line is the harmonic ICVT/μOMT results from ref 12.

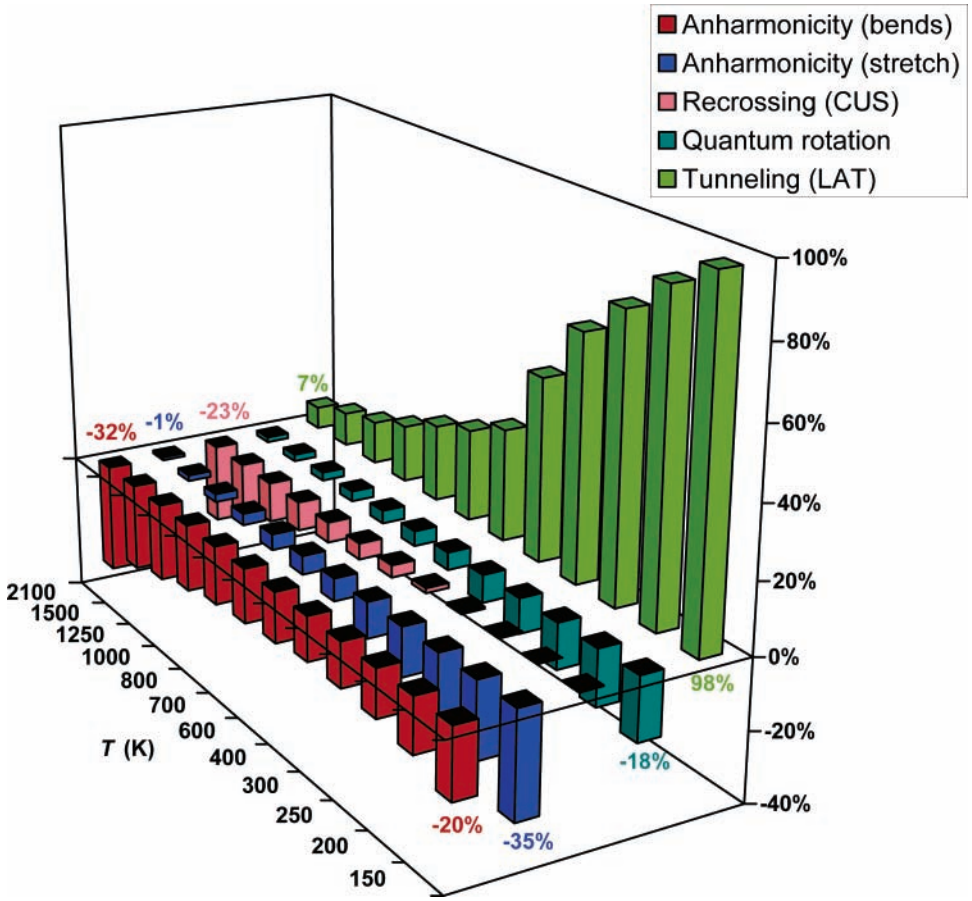

Figure 7. Percentage change in the rate constants from harmonic ICVT calculations with classical rotational partition functions upon including anharmonicity in the bends (centrifugal oscillator approximation), anharmonicity in the stretch (WKB approximation), recrossing factor (CUS approximation), quantum rotational partition functions, and tunneling (LAT approximation).

In brief, VTST/ST results agree very well with quantal accurate values even when the harmonic approximation is used and tunneling is computed using the μOMT method. This can be seen from the small values of the mean errors in Table 4 (computed as the height of the rectangle whose area is the same as the unsigned area under the curve in Figure 6).

5. Conclusions

A detailed analysis of the influence of different factors on the accuracy of thermal rate constants calculated by transition state theory allows us to learn which the weakest points of this method are and how to improve its performance. To carry out such analysis we need a realistic potential energy surface and accurate results to compare to. The reaction $H_2 + Cl \rightarrow HCl + H$ fulfills these requirements.

Figure 7 summarizes the influence of the anharmonicity, recrossing, tunneling, and quantum effects on the rotational partition functions. Our results show that anharmonicity has a significant effect, so that the differences between VTST/ST and quantal rates are about 50% smaller when anharmonicity is included. Nevertheless, the harmonic results are also reasonably reliable. On the other hand, the LCT4 method, which is supposed to improve the LCT3 results when vibrations are treated as harmonic, underestimate the magnitude of the tunneling effect. Thus, the LCT3 method works better than LCT4 either treating the vibrations harmonically or anharmonically.

Recrossing effects have negligible effect on the reaction dynamics, although it may be appreciable at high temperatures. Tunneling, however, is very important. The agreement between ICVT/LAT and quantal rates at 150 K, where 98% of the reaction goes by tunneling, is very encouraging. The LCT3 and μOMT (based on LCT3) methods for tunneling are also quite accurate above 200 K, where 93% of the reaction occurs by tunneling.

However, a special advantage of transition state theory is that it can be applied to large-size systems, including enzymatic reactions.[23,47] It is therefore interesting to extrapolate our findings to the calculation of large systems.

Anharmonicity of the vibrational modes which are not directly involved in the reaction have a negligible effect on the rate constants. The anharmonicity of the modes which correspond to free translations and vibrations that evolve to vibrations (usually called transitional modes), such as the bending modes in this reaction, or the anharmonicity of the mode directly involved in the reaction, such as the stretching mode in our study, largely contribute to the rate. Our calculations show that the separable-mode approximation seems to be very reliable, the anharmonicity of the bending modes may have an important effect on the rate constant, and anharmonicity of the stretching mode have a significant effect on conventional transition state theory rate constants, although most of its effect is due to the anharmonicity of the H_2 stretch. Moreover, the anharmonicity of the stretch at the variational transition state cancels out the anharmonicity of the H_2, and the harmonic approximation for the stretch works well for variational transition state theory. With respect to large-size systems, we can also expect some compensation in the stretch anharmonicity and, therefore, the anharmonicity of the transitional modes will have the largest effect on the rate constants. Thus, if the transition state has very

low transitional frequencies (for example, loose transition states), then anharmonicity can have a large impact on rate constants.[46,48]

For this reaction we found that, as expected, recrossing can be neglected. However, recrossing and related nonequilibrium effects may be important for reactions in large-size systems, when the dynamics of the environment are slow on the time scale over which the transition state is crossed. A reactant-like environment can push the system back toward reactants after having crossed the transition state. The study of small systems is not able to provide satisfactory conclusions with regard to recrossing and nonequilibrium effects in large systems; this is an issue that requires further study.

Tunneling is very important for reactions involving a light atom transfer. We have seen that the LCT4 method is unable to deal with the problems of the LCT3 method associated with anharmonicity. The LCT4 method adds a correction to the effective tunneling energy along the nonadiabatic region of the tunneling path, but it seems that the problem of the harmonic LCT3 method is the location of the boundaries between the adiabatic and nonadiabatic zones. We conclude that the LCT4 method is less reliable than LCT3 under the harmonic approximation, although further work is needed to settle this point. On the other hand, the LAT approximation is more reliable than the μOMT method at very low temperatures for this reaction. In general, we can expect that when the μOMT tunneling factor differs significantly from both the SCT and LCT3 factors, the angle between the reaction path and the tunneling path largely depends on the tunneling energy, and the μOMT method may be underestimating tunneling effects.

Finally, variational transition state with semiclassical tunneling coefficients under the harmonic approximation can be expected to provide reasonably accurate rate constants for the $H_2 + Cl$ reaction. Thus, our results give us confidence in the values given in ref 12.

Acknowledgment. The authors would like to thank Professors Uwe Manthe and Wensheng Bian for providing us with the results from refs 11 and 12. We would also like to thank Professor Hans-Joachim Werner for providing us with a copy of the FORTRAN code for their analytical potential energy function of ref 9, as well as Professors Donald G. Truhlar for his provision of the Polyrate 9.3 and Abcrate 10.0 programs, and Kieran F. Lim for his provision of the Mariner code.

References and Notes

(1) Corchado, J. C.; Chuang, Y.-Y.; Fast, P. L.; Villà, J.; Hu, W.-P.; Liu, Y.-P.; Lynch, G. C.; Nguyen, K. A.; Jackels, C. F.; Melissas, V. S.; Lynch, B. J.; Rossi, I.; Coitiño, E. L.; Fernandez-Ramos, A.; Pu, J.; Albu, T. V.; Steckler, R.; Garrett, B. C.; Isaacson, A. D.; Truhlar, D. G. POLYRATE-version 9.3, University of Minnesota, Minneapolis, 2003. http://comp.chem.umn.edu/polyrate.

(2) Garrett, B. C.; Lynch, G. C.; Allison, T. C.; Truhlar, D. G. ABCRATE-version 10.0, University of Minnesota: Minneapolis, MN, 1997. http://comp.chem.umn.edu/abcrate.

(3) Smedarchina, Z.; Fernández-Ramos, A.; Siebrand, W. *J. Comput. Chem.* **2001**, *22*, 787.

(4) According to the Current Contents database, 14 papers were published during the last six months of 2004 comparing transition state theory and experimental rate constants or kinetic isotope effects. In general, good agreement is found.

(5) Truhlar, D. G.; Kuppermann, A. *Chem. Phys. Lett.* **1971**, *9*, 269.

(6) Truhlar, D. G.; Merrick, J. A.; Duff, J. W. *J. Am. Chem. Soc.* **1976**, *98*, 6771.

(7) Allison, T. C.; Truhlar, D. G. In *Modern Methods for Multidimensional Dynamics Computations in Chemistry*; World Scientific: Singapore, 1998; p 618.

(8) Bian, W.; Werner, H.-J. *J. Chem. Phys.* **2000**, *112*, 220.

(9) Capecchi, G.; Werner, H.-J. *Phys. Chem. Chem. Phys.* **2004**, *6*, 4975.

(10) Manthe, U.; Capecchi, G.; Werner, H.-J. *Phys. Chem. Chem. Phys.* **2004**, *6*, 5026.

(11) Manthe, U.; Bian, W.; Werner, H.-J. *Chem. Phys. Lett.* **1999**, *313*, 647.

(12) Wang, M.; Bian, W. *Chem. Phys. Lett.* **2004**, *391*, 354.

(13) Mielke, S. L.; Allison, T. C.; Truhlar, D. G.; Schwenke, D. W. *J. Phys. Chem.* **1996**, *100*, 13588.

(14) Skokov, S.; Zou, S.; Bowman, J. M.; Allison, T. C.; Truhlar, D. G.; Lin, Y.; Ramachandran, B.; Garrett, B. C.; Lynch, B. J. *J. Phys. Chem. A* **2001**, *105*, 2298.

(15) Xie, T.; Bowman, J. M.; Peterson, K. A.; Ramachandran, B. *J. Chem. Phys.* **2003**, *119*, 9601.

(16) Koizumi, H.; Schatz, G. C.; Gordon, M. S. *J. Chem. Phys.* **1991**, *95*, 6421.

(17) (a) Huarte-Larrañaga, F.; Manthe, U. *J. Chem. Phys.* **2000**, *113*, 5115. (b) Huarte-Larrañaga, F.; Manthe, U. *J. Phys. Chem. A*, **2001**, *105*, 2522. (c) Bowman, J. M.; Wang, D.; Huang, X.; Huarte-Larrañaga, F.; Manthe, U. *J. Chem. Phys.* **2001**, *114*, 9683. (d) Wu, T.; Werner, H.-J.; Manthe, W. *Science* **2004**, *306*, 2227.

(18) Jordan, M. J. T.; Gilbert, R. G. *J. Chem. Phys.* **1995**, *102*, 5669.

(19) Espinosa-García, J.; Corchado, J. C. *J. Phys. Chem.* **1996**, *100*, 16561.

(20) (a) Pu, J.; Corchado, J. C.; Truhlar, D. G. *J. Chem. Phys.* **2001**, *115*, 6266. (b) Pu, J.; Truhlar, D. G. *J. Chem. Phys.* **2002**, *117*, 1479.

(21) Huarte-Larrañaga, F.; Manthe, U. *J. Chem. Phys.* **2002**, *117*, 4635.

(22) Espinosa-García, J.; García-Bernáldez, J. C. *Phys. Chem. Chem. Phys.* **2000**, *2*, 2345.

(23) Truhlar, D. G.; Gao, J.; Garcia-Viloca, M.; Alhambra, C.; Corchado, J. C.; Sánchez, M. L.; Poulsen, T. D. *Int. J. Quantum Chem.* **2004**, *100*, 1136.

(24) Fukui, K. In *The World of Quantum Chemistry*; Daudel, R., Pullman, B., Eds.; Reidel: Dordrecht, The Netherlands, 1974; p 113.

(25) Villá, J.; Truhlar, D. G. *Theor. Chem. Acc.* **1997**, *97*, 317.

(26) Fast, P. L.; Truhlar, D. G. *J. Chem. Phys.* **1998**, *109*, 3721.

(27) Jackels, C. F.; Gu, Z.; Truhlar, D. G. *J. Chem. Phys.* **1995**, *102*, 3188.

(28) Miller, W. H.; Handy, N. C.; Adams, J. E. *J. Chem. Phys.* **1980**, *72*, 99.

(29) Garrett, B. C.; Truhlar, D. G. *J. Chem. Phys.* **1984**, *81*, 309.

(30) Truhlar, D. G.; Isaacson, A. D.; Garrett, B. C. In *Theory of Chemical Reaction Dynamics*; Baer, M., Ed.; CRC Press: Boca Raton, FL, 1985; Vol. 4, p 65.

(31) (a) Garrett, B. C.; Truhlar, D. G. *J. Phys. Chem.* **1979**, *83*, 1915. (b) Garrett, B. C.; Truhlar, D. G. *J. Phys. Chem.* **1991**, *95*, 10374.

(32) Hase, W. L.; Lim, K. F. Mariner program, 1996; http://www.deakin.edu.au/~lim.

(33) Hase, W. L.; Duchovic, R. J.; Hu, X.; Komornicki, A.; Lim, K. F.; Lu, D.-H.; Peslherbe, G. H.; Swamy, K. N.; Vande Linde, S. R.; Varandas, A.; Wang, H.; Wolf, R. J. *QCPE Bull.* **1996**, *16*, 43.

(34) Garrett, B. C.; Truhlar, D. G. *J. Chem. Phys.* **1982**, *76*, 1853.

(35) Miller, W. H. *J. Chem. Phys.* **1982**, *76*, 4904.

(36) Skodje, R. T.; Truhlar, D. G. *J. Phys. Chem.* **1981**, *85*, 624.

(37) Marcus, R. A.; Coltrin, M. E. *J. Chem. Phys.* **1977**, *67*, 2609.

(38) Lu, D.-h.; Truong, T. N.; Melissas, V. S.; Lynch, G. C.; Liu, Y.-P.; Garrett, B. C.; Steckler, R.; Isaacson, A. D.; Rai, S. N.; Hancock, G. C.; Lauderdale, J. G.; Joseph, T.; Truhlar, D. G. *Comput. Phys. Commun.* **1992**, *71*, 235.

(39) Liu, Y.-P.; Lynch, G. C.; Truong, T. N.; Lu, D.-h.; Truhlar, D. G. *J. Am. Chem. Soc.* **1993**, *115*, 2408.

(40) Truong, T. N.; Lu, D.-h.; Lynch, G. C.; Liu, Y.-P.; Melissas, V. S.; Stewart, J. J. P.; Steckler, R.; Garrett, B. C.; Isaacson, A. D.; Gonzalez-Lafont, A.; Rai, S. N.; Hancock, G. C.; Joseph, T.; Truhlar, D. G. *Comput. Phys. Comm.* **1993**, *75*, 143.

(41) Fernández-Ramos, A.; Truhlar, D. G. *J. Chem. Phys.* **2001**, *114*, 1491.

(42) Garrett, B. C.; Truhlar, D. G. *J. Chem. Phys.* **1983**, *79*, 4931.

(43) Garrett, B. C.; Abusalbi, N.; Kouri, D. J.; Truhlar, D. G. *J. Chem. Phys.* **1985**, *83*, 2252.

(44) Liu, Y.-P.; Lu, D.-h.; Gonzalez-Lafont, A.; Truhlar, D. G.; Garrett, B. C. *J. Am. Chem. Soc.* **1993**, *115*, 7806.

(45) Garrett, B. C.; Truhlar, D. G.; Grev, R. S.; Magnuson, A. W. *J. Phys. Chem.* **1980**, *84*, 1730. Erratum: *J. Phys. Chem.* **1983**, *87*, 4554.

(46) Truhlar, D. G.; Garrett, B. C.; Klippenstein, S. J. *J. Phys. Chem.* **1996**, *100*, 12771.

(47) García-Viloca, M.; Gao, J.; Karplus, M.; Truhlar, D. G. *Science* **2004**, *303*, 186.

(48) Espinosa-García, J.; Corchado, J. C. *J. Phys. Chem. A* **1997**, *101*, 7336.